Ortega, Pablo; Garin, Moises; von Gastrow, Guillaume; Savisalo, Tuukka; Tolvanen, Antti; Vahlman, Henri; Vähänissi, Ville; Pasanen, Toni; Carrio, David; Savin, Hele; Alcubilla, Ramon

Black silicon back contact module with wide light acceptance angle

Published in:
Progress in Photovoltaics

DOI:
10.1002/pip.3231

Published: 01/03/2020

Document Version
Peer reviewed version

Please cite the original version:
Ortega, P., Garin, M., von Gastrow, G., Savisalo, T., Tolvanen, A., Vahlman, H., Vähänissi, V., Pasanen, T., Carrio, D., Savin, H., & Alcubilla, R. (2020). Black silicon back contact module with wide light acceptance angle. *Progress in Photovoltaics*, *28*(3), 210-216. https://doi.org/10.1002/pip.3231

Black silicon back contact module with wide light acceptance angle

Pablo Ortega[1], Moises Garín[1,2], Guillaume von Gastrow[3], Tuukka Savisalo[4], Antti Tolvanen[5], Henri Vahlman[5], Ville Vähänissi[6], Toni P. Pasanen[6], David Carrió[1], Hele Savin[6], Ramón Alcubilla[1]

[1] Universitat Politècnica de Catalunya, Micro and NanoTechnologies (MNT) group, Jordi Girona 1-3 Modul C-4, E – 08034 Barcelona, Spain

[2] GR-MECAMAT, Universitat de Vic – Universitat Central de Catalunya (UVIC-UCC), Campus Torre dels Frares, c/ de la Laura 13, 08500 Vic, Spain.

[3] Now in Department of Nanoengineering, University of California, San Diego, La Jolla, California 92093, United States

[4] Valoe Oyj, Insinöörinkatu 5, FI-50150 Mikkeli, Finland

[5] Endeas Oy, Ruukinkuja 1, 02330 Espoo, Finland

[6] Aalto University, Department of Electronics and Nanoengineering, Tietotie 3, 02150 Espoo, Finland

Abstract

In this work a photovoltaic mini-module combining interdigitated back contacted solar cells with black silicon in the front was implemented as a proof of concept. The module consists of nine solar cells connected in series with an active area of 86.5 cm^2. Both the assembly and panel encapsulation were made using industrial back contact module technology. Noticeable photovoltaic efficiencies of 18.1% and 19.9% of the whole module and the best individual cell of the module respectively, demonstrate that fragile nanostructures can withstand standard module fabrication stages. Open circuit voltage and fill factor values of 5.76 V and 81.6% respectively reveal that series interconnection between cells works as expected, confirming a good ohmic contact between cell busbars and the conductive back sheet. Additionally, the excellent quasi-omnidirectional anti-reflection properties of black silicon surfaces prevails at module-level, as it is corroborated by light incidence angle dependence measurements of the short circuit current parameter.

Keywords: black silicon, interdigitated back contact solar cell, surface passivation, module, encapsulation.

1. Introduction

Black silicon (b-Si) etching has become a common technique to reduce drastically reflectance on silicon based solar cells and other photovoltaic devices rendering the surface visibly black [1, 2]. The near-zero reflectance is achieved by the nanostructures due to a gradual refraction index variation from the air to the silicon. Another important advantage of b-Si is the low incidence light angle dependence of surface reflectance increasing the daily, monthly and yearly PV energy production independently of the location latitude [3].

Black silicon surfaces can be achieved using different techniques which can be easily incorporated in the PV industry such as metal-assisted wet-chemical etching (MACE), dry reactive ion etching (RIE), inductive couple plasma-reactive ion etching (ICP-RIE), laser structuring and electrochemical etching [4]. Additionally, collateral benefits of b-Si have arisen recently improving low-cost substrates by removing saw surface damage in diamond-wire-sawn (DWS) wafers [5], or increasing the gettering effect during doping diffusion on CZ c-Si solar cells [6]. All these advantages make black silicon etching a very attractive candidate to replace conventional acidic and alkaline texturizing approaches in the PV fabrication chain. For instance, in ref. [7] is demonstrated the economic viability of replacing acidic texturing by ICP-RIE b-Si nanostructures using a convectional industrial process based on mc-Si substrates.

One of the major drawbacks of b-Si is the difficulty to passivate the textured surface because of the high aspect ratio of nanostructures and the increase of Auger recombination in doped b-Si regions due to high doping concentrations [8]. In the last years many efforts have been applied to obtain low recombination black silicon surfaces using either doped or non-doped nanostructures [9-12]. For instance, MACE etching technique has been successfully applied to large-area both-side contacted DWS mc-Si or CZ c-Si solar cells with efficiencies over 19% using phosphorous doped b-Si passivated with plasma-enhanced chemical vapor deposition (PECVD) SiN_x [5,13].

Alternatively, a back contacted solar cell structure is more well suited to reach high efficiency devices since it avoids both front grid metallization shadowing and high Auger recombination near the front surface, i.e. high doped regions are placed at the rear side.

An additional advantage of this type of solar cell concept is the facility to assemble solar cells in modules provided a coplanar connection. With this idea in mind, record efficiencies (22.1%) have been reported using an interdigitated back contacted (IBC) solar cell architecture (9 cm^2) on p- and n-type c-Si substrates [14, 15]. In this approach, a non-doped b-Si in the front surface was passivated using very conformal annealed Al_2O_3 layers deposited by the atomic layer deposition (ALD) technique reaching surface recombination velocities below ~10 cm/s independently of the substrate polarity [16].

These results, using either a both-side or a back contacted cell architecture, pave the way for introducing b-Si to obtain high efficiency and cost-effective devices. Indeed, silicon based solar cell manufacturers already apply b-Si in their products based on both-side contacted structures using MACE technology [17-19]. However, there are no reported studies in the scientific literature about black back contact PV modules. Therefore, it is important to elucidate back-contact solar cell behavior at module level and to test, for instance, if fragile b-Si nanostructures fabricated by RIE can withstand conventional assembly and encapsulation processes typically used in the PV industry.

In this work, we explore the compatibility of b-Si with traditional module processing, fabricating a black mini-module (~ 100 cm^2) based on IBC c-Si(n) solar cells and using encapsulation and assembly processes which are routinely used in standard back contacted modules [20, 21]. Individual cells were characterized before and after encapsulation. Full module measurements were also done including the influence of the light incidence angle on the short-circuit current parameter. In addition, the impact of the encapsulation glass quality in the photovoltaic performance was also analyzed, i.e. solar grade glass with or without antireflection coating (ARC) layer. A module efficiency of 18.1% with individual solar cell efficiencies up to 19.9%, demonstrate the viability of b-Si, together with IBC solar cells and industrial encapsulation processes to reach high efficiency black back contact modules.

2. IBC solar cells

2.1 Fabrication

Interdigitated back-contacted solar cells where fabricated on 4 inch float zone (FZ) c-Si(n) wafers (1-3 Ωcm, 260 μm thick). The choice of n-type substrates to implement the black mini-module was done based on the more stable b-Si surface passivation exhibited by this type of substrate polarity compared with the p-type counterparts as can be seen in Fig. S1a included in the Supporting Information section.

Solar cells were fabricated following a similar fabrication process as is reported in ref. [15] but using in this case strip-like regions for both contact windows and base and emitter doped regions, and an emitter coverage (f_e) of 80%, i.e. the ratio between emitter strip area and total cell area. This f_e value is chosen in order to maximize photovoltaic efficiency as a trade-off between high photocarrier collection, i.e. low electrical shadowing, and low lateral base resistance losses as can be seen in Fig. S1b included in the Supporting Information section.

The fabrication process involves the next main features/stages, namely: i) interdigitated p+, n+ and n++ doped regions at the rear side were made by convectional boron and phosphorous diffusion regions using solid planar sources and finally passivated with thermal dry SiO_2 (110 nm thick). ii) Once the SiO_2 layer was removed on the front surface, b-Si etching was made by cryogenic (-120ºC) ICP-RIE using SF_6 and O_2 as reactive gases with the process reported in [9]. iii) Next, the wafers were SC1/SC2 cleaned before the atomic layer deposition of ~20 nm thick Al_2O_3 layers at 200ºC using trimethylaluminum (TMA) and a combination of water and ozone as aluminum precursor and oxidant agent, respectively [22]. No HF dip was performed before Al_2O_3 deposition to ensure an hydrophilic surface. iv) After strip-like contact windows were opened, a 4 μm thick Al layer (first metallization level) was deposited by e-beam evaporation and patterned by photolithography to form the interdigitated back contact electrodes. v) Finally, a forming gas annealing at 400ºC for 10 min was performed to both guarantee good/reliable ohmic contacts and activate surface passivation on the b-Si front surface [16]. Additionally, this annealing stage recovers rear surface passivation, provided by the thermal SiO_2 film, from the surface damage after e-beam metallization [23].

In order to simplify the mini-module coplanar assembly and reduce the contribution in the series resistance of the rear metal electrode grid, a two-level metallization scheme was chosen at the rear side for our IBC cells as can be seen in Fig. 1. The second metallization level defines the base and emitter busbars. It consists of a stack of aluminum and silver, ~1.0 and ~0.3 µm thick films respectively, which were deposited by thermal evaporation using a metal mask at the end of the fabrication process. An intermediate structural dielectric layer of photosensitive polyimide (~ 7 µm thick) was deposited by spin coating in between the first and second metallization levels for isolation purposes. Both metallization levels were electrically connected by vias through the polyimide layer, which are patterned using standard photolithography. Before depositing the second metallization level the polyimide based interlayer was cured at 325ºC for 30 min on a hot plate with N_2 vent. Four IBC cells were fabricated in each wafer, see Fig. 1a, with an active area of 3.1×3.1 cm^2. Emitter and base wide busbars are clearly seen in the same figure with areas of 3.0×1.2 and 3.0×1.6 cm^2, respectively. A non-metallized gap between busbars of 2 mm was used to avoid any metal shunt.

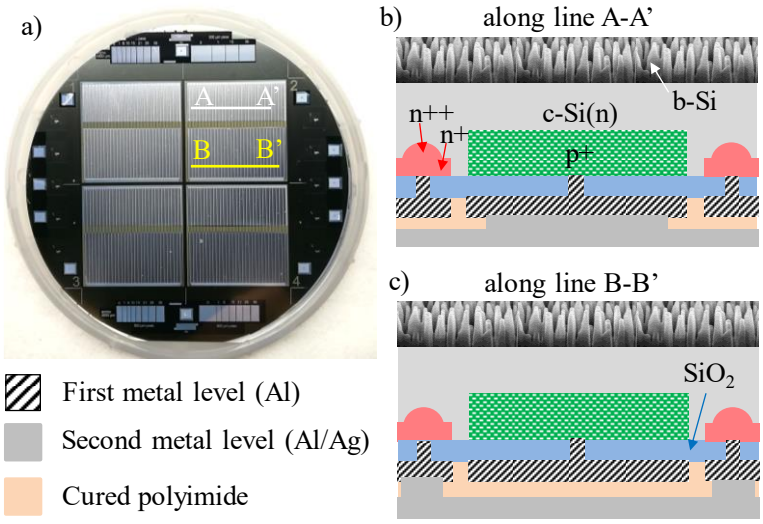

Fig. 1. a) Image of a processed 4 inch wafer (electrode/rear side view) showing four IBC solar cells, which are labelled from 1 to 4. Cross section sketches along lines b) A-A' (in the emitter busbar) and c) B-B' (in the base busbar) exhibiting the two-level metallization scheme.

One important technological issue is to quantify the impact of polyimide curing in the rear surface passivation of our finished devices. In order to assess passivation quality after polyimide curing, some test samples passivated symmetrically with thermal dry SiO_2 and ALD Al_2O_3, 110 and 20 nm thick layers, respectively, were fabricated. Next, the samples were annealed at 400 ºC (10 min) and covered on one side by the polyimide film and underwent the curing stage at 325 ºC for 30 min (see Fig. 2a). Finally, quasi-steady-state photoconductance decay (QSS-PC) lifetime measurements were performed. As it can be seen in Fig. 2b, the polyimide curing stage does not jeopardize surface passivation in any case, and surface passivation is even improved for the ALD Al_2O_3 covered sample.

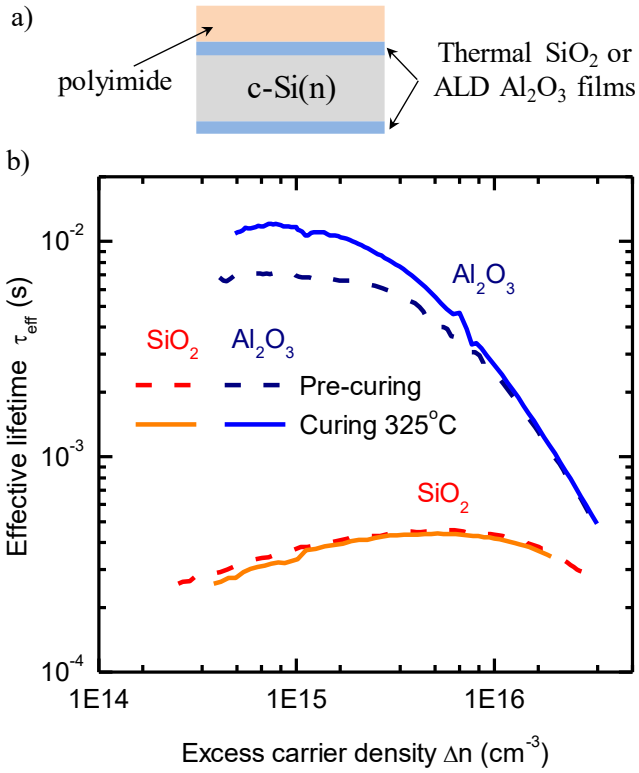

Fig. 2. a) Sketch of a symmetrical passivated test c-Si(n) sample using either thermal dry SiO_2 or ALD Al_2O_3. b) Lifetime measurements vs. carrier excess density (Δn) before (dashed lines) and after (continuous lines) the polyimide curing stage at 325 ºC 30 min for the two passivation layers.

2.2 Results before encapsulation

Once the fabrication process was finished, solar cells were measured under standard test conditions (STC, AM1.5G 1 kW/m^2 solar spectrum, T=25ºC) by means of a solar simulator (ORIEL 94021A, Newport corporation) and a current-voltage I-V source-meter (Keithley 2601B, Tektronix, Inc) using 4-probes to discard ohmic losses in the wires and measurement tips. External quantum efficiency (*EQE*) curves were extracted using the QEX10 system (PV Measurements, Inc) under a white bias light of 0.2 Suns.

Table I shows the main photovoltaic parameters of the best nine IBC solar cells from three wafers before laser wafer dicing and module assembly. Solar cells exhibit remarkable photovoltaic efficiencies (η) of about 20.5 ± 0.6% with open circuit voltage (V_{oc}) and fill factor (*FF*) of 635±10 mV and 79.7±1.2%, respectively. It is important to remark that a relatively good short-circuit current density (J_{sc}) matching (40.5 ± 0.7 mA/cm^2) is achieved. The slight variation in photocurrent values arises from small differences in the front b-Si surface passivation before wafer dicing. Fig. 3 shows the *EQE* spectra of the best and worst solar cells. By fitting experimental results with 2D simulations in the visible part of the spectrum using the front surface recombination velocity S_F as a free parameter, we can conclude that surface passivation is pretty good in all samples with S_F values in the 15-40 cm/s range. It is important to remark that *EQE* measurements were made after several weeks once the cells were fabricated. Therefore, the extracted S_F values should be very close to the stabilized ones (see Fig. S1a in the Supporting Information section). In addition, relatively low V_{oc} values are achieved in our devices, despite the excellent front surface passivation. This points out that rear recombination (base contacts, gap and emitter regions) plays an important role in the cell electrical performance by limiting V_{oc}.

Table I. Main photovoltaic parameters of IBC solar cells before wafer laser dicing under solar spectrum AM1.5G (1 kW/m^2, 25°C). The best nine devices from three different wafers (wafers labelled A, B and C) were used to the final module assembly. The best and the worst cell data are in bold and highlighted in green and red color, respectively.

Cell	J_{sc} (mA/cm^2)	V_{oc} (V)	FF (%)	η (%)
#A1	41.1	0.636	79.4	20.7
#A2	40.6	0.643	80.9	21.1
#A4	**40.8**	**0.639**	**80.8**	**21.1**
#B2	40.7	0.644	79.7	20.9
#B3	40.2	0.637	79.9	20.5
#B4	40.4	0.642	80.4	20.8
#C1	40.0	0.634	79.4	20.1
#C3	**39.8**	**0.625**	**80.0**	**19.9**
#C4	40.3	0.631	78.5	19.9

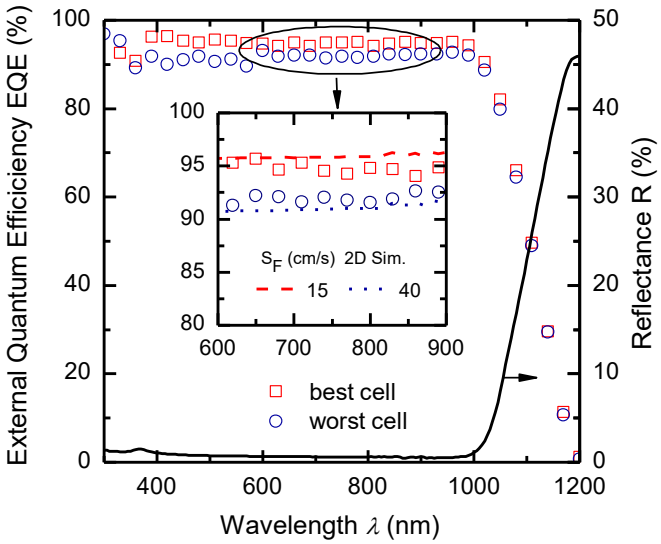

Fig. 3. *EQE* curves (symbols) for the best and worst IBC cells used to fabricate the module (before wafer dicing). Dashed and dotted color lines presented in the inset correspond with 2D simulations considering two S_F representative values to fit the *EQE* curves. Reflectance measured in a finished IBC cell is also included in the graph (continuous black line).

3. IBC module

3.1 Assembly and encapsulation

The black silicon module consists of nine IBC solar cells (whose characteristics are listed in table I) that are connected in series resulting in a total useful photovoltaic module area of 86.5 cm^2. Assembly and encapsulation was made using conventional back contact technology [24]. The series connection between cells was done by placing solar cells on a conductive back sheet plane with 35 μm thick copper metallization interconnections in a serpentine-like fashion as can be seen in Fig. 4a. The copper interconnection was designed in a manner that allowed the measurement of either all of the cells individually or the whole module at once.

Single solar cells were cut out from the wafers by means of laser wafer dicing using a fiber laser (1024 nm) with approximately 30 μm beam size. A security gap of 500 μm was used between the cell active area and the center of the laser dice paths both to take alignment inaccuracy into account and to minimize the impact of laser damage during dicing on electrical module performance.

The assembly was sandwiched between two 3.2 mm ARC-free solar grade glasses with polyolefin based encapsulant. The contact between the cell and the conductive back sheet was done using commercial electrically conductive adhesive (ECA) that is designed for back contact module interconnection.

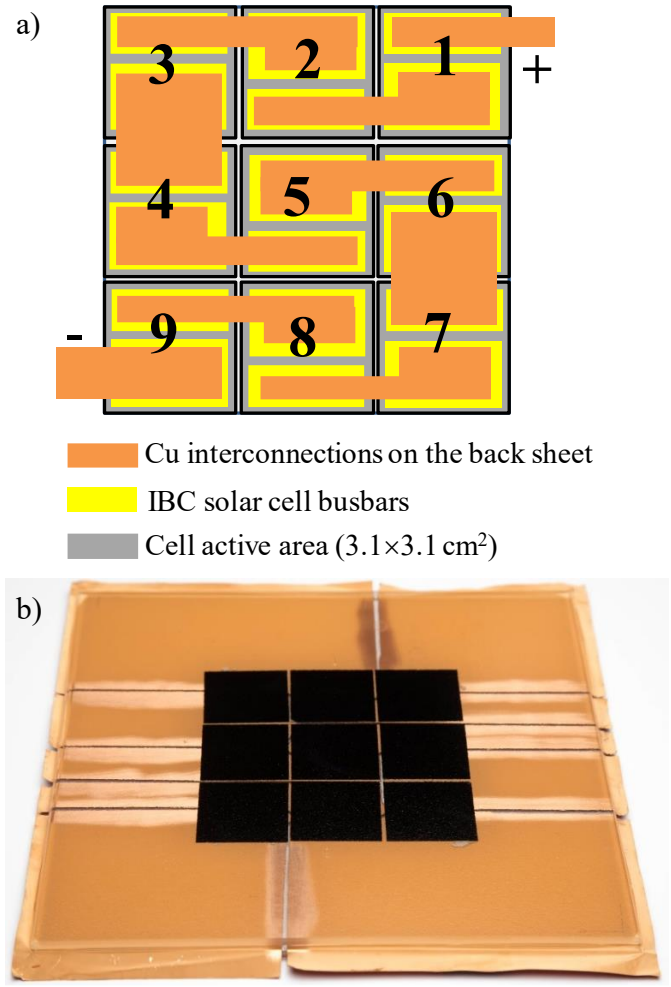

Fig. 4. a) Simplified scheme of the interconnection between cells in the mini-module (cell back side view). 9 cells are assembled in series and labelled from 1 to 9. b) Front view of the fabricated b-Si IBC module as a proof of concept (active area 86.5 cm^2).

It is important to remark that no relevant morphological damage and/or scratches of nanostructures was observed after finishing the module keeping the original black surface appearance (see Fig. 4b) without apparent bubbles or voids in the encapsulant. A similar result was reported in a previous work using a single-cell encapsulated module but using in this case a b-Si PERC-like solar cell [25].

3.2 Characterization of encapsulated cells and module

Photovoltaic parameters, at module level, were measured using a Quicksun 800-series class AAA module solar simulator under standard test conditions (AM1.5G solar spectrum 1 kW/m^2 25ºC). The measurement set-up system also allows to characterize the module performance for different light incidence angles. This was implemented by fixing the panel on a rotating stage and determining the angle of rotation of the module with respect to the center of the light source. Since both the diameter of the module (13.4 cm) and the radius of the light source (< 13 cm) are small compared to the distance between the light source and the module (> 5 m), all the light falls on the panel surface at an incident angle of < 2.3° when the rotation angle is set to 0°. Hence, the error arising from non-parallel light is expected to be small.

The current-voltage (*I-V*) and power-voltage (*P-V*) curves of the final module are shown in Fig. 5. Table II summarizes photovoltaic parameters for the whole module and for each single cell.

As can be seen in table II, a remarkable efficiency of 18.1% has been achieved for the whole module and near 20% for the best cell of the panel. The open circuit voltage of the module of about 5.76 V points out that the voltage scaling up provided by the series connection works properly, i.e. the total V_{oc} corresponds to the sum of all single cell values. Moreover, the relatively high *FF* value (over 81%) of the module confirms a good and reliable connection between cell busbars and the copper-based metal interconnection backsheet after module assembly.

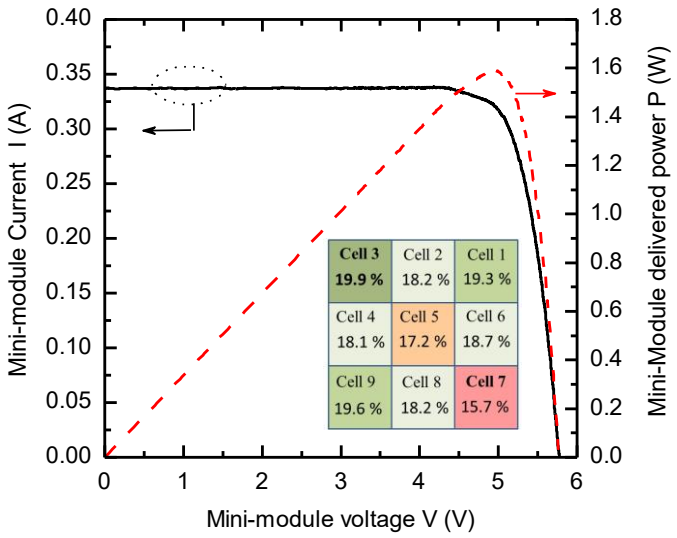

Fig. 5. Current- and power-voltage characteristics of the mini-module under AM1.5G solar spectrum (1 kW/m^2, 25°C). Efficiency mapping for each IBC solar cell is shown in the inset, where dark-green and red filled cells are the best and worst cells of the module.

Table II. Photovoltaic parameters for each assembled solar cell and for the whole module. Measurements were made under STC conditions. The best and worst encapsulated cell data considering the J_{sc} parameter are in bold and highlighted in green and red color, respectively.

Cell	I_{sc} (mA)	J_{sc} (mA/cm^2)	V_{oc} (V)	FF (%)	η (%)
#1	363	37.8	0.648	78.9	19.3
#2	350	36.4	0.633	78.7	18.2
#3	**375**	**39.0**	**0.645**	**79.1**	**19.9**
#4	354	36.8	0.641	79.0	18.7
#5	**333**	**34.6**	**0.627**	**79.6**	**17.2**
#6	343	35.7	0.642	79.0	18.1
#7	336	35.0	0.633	71.0	15.7
#8	355	36.9	0.634	77.4	18.2
#9	368	38.3	0.644	79.5	19.6
Total	**333**	**--**	**5.760**	**81.6**	**18.1**

By comparing results from table I and II, the most affected parameter after module fabrication is the short circuit current density with average values from 40.4 to 36.7 mA/cm^2 before and after encapsulation, respectively. Part of the J_{sc} losses are caused by the front glass reflectance, which are estimated to be around 5% absolute, i.e. 2 mA of the total 4 mA drop in current from cell to module. However, in order to explain the high scattering between J_{sc} values another source of photocurrent losses needs to be considered. Concretely, an increase of bulk and surface recombination at the device edges after laser dicing, i.e. damage induced during the laser stage, might explain in part such different J_{sc} values. This problem is less important when the cell area is large, but in small devices, where the ratio between area and perimeter is high, it can be very relevant. Notice that the whole module short circuit current is limited by the lowest I_{sc} value measured from each single cell. Therefore, a non-uniform short circuit current distribution between cells will cause a dramatic drop in module efficiency. The mismatching in the short circuit current density parameter of our cells is in agreement with the apparent high *FF* of around 81.6% achieved at module level, despite single *FF* values are below 80% (see Fig. S2 in the Supporting Information section).

3.3 Photovoltaic performance at different light incidence angles

One key point in module performance is the dependence of I_{sc} on the light incidence angle (θ), i.e. $I_{sc}(\theta)$. Fig.6 shows the $I_{sc}(\theta)$ of the module, normalized with respect to the normal incidence value $I_{sc}(0^o)$. Curves are corrected considering the cosine term, $1/\cos(\theta)$, which takes the decrement of irradiance with incidence angles > 0º into account. It is important to remark that in this module prototype non-tempered ARC-free solar-quality glass was used due to challenges in cutting tempered glass to fit the small area of the mini-module. However, for comparison purposes, we have included in the graph two additional measurements using single b-Si IBC cells: a measurement from a non-encapsulated cell considering data from ref. [14], and a single-cell module, which was encapsulated in the same way as the mini-module but using in this case antireflection coated PV quality glass. In this latter case, b-Si IBC cells were fabricated in a previous work [15], exhibiting efficiencies up to 22% before encapsulation.

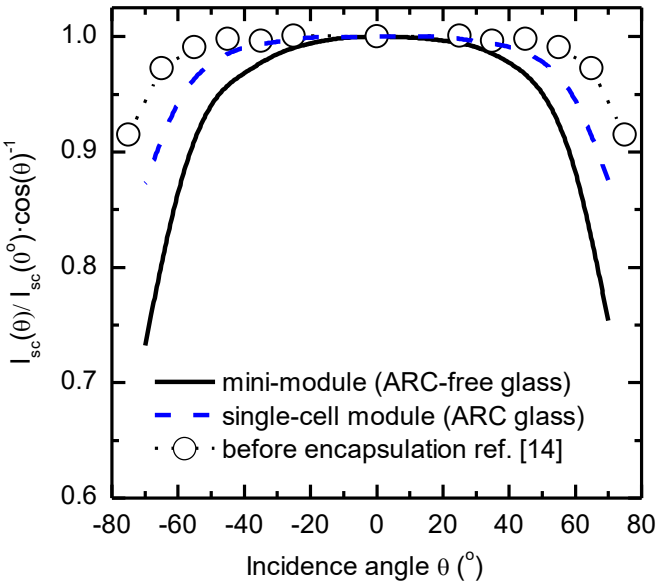

Fig.6. Normalized I_{sc} vs. light incident angle of the mini-module (continuous line). ARC-free solar grade glass was used in the module prototype fabrication. A single-cell module with ARC solar glass and a non-encapsulated single cell, both using b-Si IBC cells, were also measured (dashed lines without and with symbols respectively).

As can be seen in Fig. 6, the best results occur for the non-encapsulated cell in agreement with ref. [3]. However, normalized short circuit current losses are lower than 5% for incident angles in the -50 to 50º range in the black mini-module and could be even lower using an antireflection coated PV-quality glass, i.e. <5% losses in the $-60º < \theta < 60º$ range.

4. Conclusions

In this work a black back contact mini-module was fabricated. The module prototype consists of nine IBC solar cells connected in series with an active area of 86.5 cm^2. Assembly and encapsulation stages have used convectional processes employed routinely on industrial back contact module technologies. An open circuit voltage V_{oc} of 5.76 V confirms the voltage scaling up provided by the series connection reaching final photovoltaic efficiencies over 18% under standard test conditions. Moreover, black silicon nanostructures are preserved after fabrication stages maintaining the typical black front surface appearance on the final module. The influence of the light incidence angle

in the short circuit current has been also studied in this work corroborating the benefits of b-Si combined with a good antireflection coated glass to improve the module performance when light is not perpendicular to the panel. These results pave the way to use black silicon in the near future combined with back contacted interdigitated cells in the PV fabrication chain to achieve high efficiency and high-performance modules.

Acknowledgments

This work was partially supported by the Spanish MINECO (PCIN-2014-055) and Finnish TEKES (40329/14) agencies under Solar-Era.Net FP7 European Network. M. G. and P.O acknowledge financial support from the Spanish Ministry of Economy and Competitiveness (MINECO) through the project ENE2015-74009-JIN, co-funded by the European Regional Development Fund. A part of the work was also supported by the project REFER COMRDI15-1-0036 funded by ACCIÓ and the European Regional Development Fund (FEDER). Part of the research was performed at the Micronova Nanofabrication Centre, supported by Aalto University.

References

[1] Huang Y-F, Chattopadhyay S, Jen Y-J, Peng C-Y, Liu T-A, Hsu Y-K, Pan C-L, Lo H-C, Hsu C-H, Chang Y-H, Lee C-S, Chen K-H, Chen L-C. Improved broadband and quasi-omnidirectional anti-reflection properties with biomimetic silicon nanostructures. *Nature Nanotechnology* 2007; **2**: 770-774.

[2] Lv J, Zhang T, Zhang P, Zhao Y, Li S. Review application of nanostructured black silicon. *Nanoscale Research Letters* 2018; **13**: 110.

[3] Haedrich I, Ernst M, Thomson A, Zheng P, Zhang X, Jin H, Macdonald D. How cell textures impact angular cell-to-module ratios and the annual yield of crystalline solar modules. *Solar Energy Materials & Solar Cells* 2018; **183**: 181-192.

[4] Otto M, Algasinger M, Branz H, Gesemann B, Gimpel T, Füchsel K, Käsebier T, Kontermann S, Koynov S, Li X, Naumann V, Oh J, Sprafke AN, Ziegler J, Zilk M, Wehrspohn RB. Black silicon photovoltaics. *Advanced Optical Materials* 2015; **3**: 147-164.

[5] Su G, Dai X, Tao K, Sun H, Jia R, Jin Z, Liu X, Liu H, Liu S, Xu C, Cao Y, Zhao Y, Qu H, Liu B, Chen B. The study of the defect removal etching of black silicon for diamond wire sawn multi-crystalline silicon solar cells. *Solar Energy* 2018; **170**: 95-101.

[6] Pasanen TP, Laine HS, Vähänissi V, Schön J, Savin H. Black silicon significantly enhances phosphorus diffusion gettering. *Scientific reports* 2018; **8**: 1991.

[7] Modanese C, Laine HS, Pasanen TP, Savin H, Pearce JM. Economic advantages of dry-etched black silicon in passivated emitter rear cell (PERC) photovoltaic manufacturing. *Energies* 2018; **11**: 2337.

[8] Von Gastrow G, Ortega P, Alcubilla R, Husein H, Nietzold T, Bertoni M, Savin H. Recombination processes in passivated boron-implanted black silicon emitters. *Journal of Applied Physics* 2017; **121**: 185706.

[9] Repo P, Haarahiltunen A, Sainiemi L, Yli-Koski M, Talvitie H, Schubert MC, Savin H. Effective passivation of black silicon surfaces by atomic layer deposition. *IEEE Journal of Photovoltaics* 2013; **3**: 90-94.

[10] Jia X, Zhou C, Wang W. Optimization of the surface structure on black silicon for surface passivation. *Nanoscale Research Letters* 2017; **12**: 193.

[11] Repo P, Benick J, Von Gastrow G, Vähänissi V, Heinz FD, Schön J, Schubert MC, Savin H. Passivation of black silicon boron emitters with atomic layer deposited aluminum oxide. *Physica Status Solidi RRL* 2013; **7**(11): 950-954.

[12] Van de Loo BWH, Ingenito A, Verheijen MA, Isabella O, Zeman M, Kessels WMM. Surface passivation of n-type doped black silicon by atomic-layer-deposited SiO_2/Al_2O_3 stacks. *Apply Physic Letters* 2017; 110: 263106.

[13] Li P, Wei Y, Zhao Z, Tan X, Bian J, Wang Y, Lu C, Liu A. Highly efficient industrial large-area black silicon solar cells achieved by surface nanostructured modification. *Applied Surface Science* 2015; **357**; 1830-1835.

[14] Savin H, Repo P, Von Gastrow G, Ortega P, Calle E, Garín M, Alcubilla R. Black silicon solar cells with interdigitated back-contacts achieve 22.1% efficiency. *Nature Nanotechnology* 2015; **10**: 624-628.

[15] Ortega P, Calle E, Von Gastrow G, Repo P, Carrió D, Savin H, Alcubilla R. High-efficiency black silicon interdigitated back contacted solar cells on p-type and n-type c-Si substrates. *Progress in Photovoltaics*: *Research and Applications* 2015; **23**: 1448-1457.

[16] Calle E, Ortega P, Von Gastrow G, Martín I, Savin H, Alcubilla R. Long-term stability of Al_2O_3 passivated black silicon. *Energy Procedia* 2016; 92: 341-346.

[17] Yingli Solar. *YGE 72 Cell Series 2 Black Silicon*. Accessed: July, 12, 2019. [Online]. Available: www.yinglisolar.com/us/products/82

[18] Trinasolar. *Black silicon solar modules: A powerful and pleasing design*. Accessed: July, 12, 2019. [Online]. Available: www.trinasolar.com/us/resources/blog/black-silicon-solar-modules-powerful-and-pleasing-design

[19] PV magazine. *Suntech's black silicon solar cells enter mass production.* Accessed: July, 12, 2019. [Online]. Available: www.pv-magazine.com/2018/01/04/suntechs-black-silicon-solar-cells-enter-mass-production

[20] Van Kerschaver E, Beaucarne G. Back-contact solar cells: a review. *Progress in Photovoltaics: Research and Applications* 2006; 14: 107-123.

[21] Bennet I, Eerenstein W, Rosca V. Reducing the cost of back-contact module technology. *Energy Procedia* 2013; **38**: 329-333.

[22] Von Gastrow G, Li S, Putkonen M, Laitinen M, Sajavaara T, Savin H. Effect of ozone concentration on silicon Surface passivation by atomic layer deposited Al_2O_3. *Applied Surface Science* 2015; **357**: 2402-2407.

[23] Coll A, Martín I, Ortega P, Bermejo S, López G, Alcubilla R. Impact of metallization techniques on surface passivation of high efficiency crystalline silicon solar cells. *Proc. of 28th European Photovolatic Solar Energy Conference and Exhibition*, Paris (France), 2013; 1213–1216.

[24] Valoe. *Finnish Photovoltaic Technology*. Accessed: July, 12, 2019. [Online]. Available: www.valoe.com

[25] Pasanen TP, Vähänissi V, Wolny F, Oehlke A, Wagner M, Juntunen MA, Heikkinen ITS, Salmi E, Sneck S, Vahlman H, Tolvanen A, Hyvärinen J, Savin H. Industrial Applicability of Antireflection-Coating-Free Black Silicon on PERC Solar Cells and Modules. *Proc. of 35th European Photovolatic Solar Energy Conference and Exhibition*, Brussels (Belgium), 2018; 552–556.